

Synthesis of zeolite L membranes with sub-micron to micron thicknesses

Jeremy White^a, Prabir K. Dutta^{a,*}, Krenar Shqau^b, Henk Verweij^b

^a *Department of Chemistry, The Ohio State University, 100 W 18th Avenue, Columbus, OH 43210, USA*

^b *Department of Materials Science and Engineering, The Ohio State University, 2041 College Road, Columbus, OH 43210, USA*

Received 22 January 2008; received in revised form 12 February 2008; accepted 15 February 2008

Available online 23 February 2008

Abstract

The growth of zeolite membranes with controlled thicknesses in the sub-micron to micron region is examined, using zeolite L as the example. It was demonstrated that by controlling the concentration of the zeolite solid load and suspension viscosity, dip-coating provided a method to prepare zeolite seed layers of controlled thicknesses. Disk-shaped zeolite L crystals, with size distribution of 0.5–2 μm in diameter, were used as seed crystals for the growth of 2–7 μm thick membranes. By choosing the composition of the secondary growth medium, as well as time and temperature, crystal growth primarily occurred along the xy -plane in these micron plus-thickness membranes, with eventual thickness similar to the originally deposited seed layer. For the synthesis of sub-micron-sized membranes, seed crystals from 20 to 60 nm were used and growth was observed along the z -axis. The optimum secondary growth conditions was found to occur at 60 h of growth time (40 h for sub-micron membranes) using a temperature of 110 $^{\circ}\text{C}$ with a solution composition of $10\text{K}_2\text{O}:1\text{Al}_2\text{O}_3:20\text{SiO}_2:2000\text{H}_2\text{O}$. Membranes were characterized by electron microscopy and single gas permeation studies, providing confirmation of membrane densification.

© 2008 Elsevier Inc. All rights reserved.

Keywords: Zeolite L; Alumina; Membrane; Secondary growth; Controlled thickness

1. Introduction

Zeolites have been extensively studied for industrial applications, including catalysis, ion exchange, gas separation, nuclear waste disposal, chemical sensing and light-harvesting devices [1–6]. The preparation of supported zeolite films/membranes with controlled microstructure is attractive for a number of applications, particularly for separations and catalytic applications. In supported zeolite membranes, the support provides the required mechanical strength without imposing additional mass transfer resistance. Generally, the intercrystalline porosity [7,8], crystal size [9], crystal orientation relative to the membrane layer [10,11] and thickness and uniformity of the zeolite membranes [12] determine their performance. The framework

of the Linde type L zeolite (LTL) provides ideal geometrical properties for the arrangement and stabilization of incorporated supramolecular systems due to its one-dimensional pore structure [13,14]. To the best of our knowledge, only one report of zeolite L films/membranes has been described, in which Tsapatsis et al. prepared a nanocrystalline zeolite L/boehmite cast that was later grown into a thin, randomly oriented self-supported film [15,16]. These fragile nanocrystalline casts were converted into much larger zeolite L crystals following secondary growth.

The emphasis on the development of novel architectures for integrating photochemical molecular assemblies into practical devices for conversion of solar to chemical energy has rapidly increased due to the increasing demands of energy consumption. Dutta and Kim have demonstrated that ruthenium-based photosensitizers can be attached to the pores of zeolite Y membranes for light-harvesting reactions [17]. Since the zeolites provide the proper spatial arrangement for long-lived charge separation, it was shown

* Corresponding author. Tel.: +1 614 2924532; fax: +1 614 6885402.
E-mail address: dutta@chemistry.ohio-state.edu (P.K. Dutta).

that a sturdy zeolite membrane provided access to the photochemically generated redox species for reactions such as the conversion of water to H_2 [18]. Motivated by these demands, our current research is aimed at designing zeolite membranes with controlled thickness. In this paper, using zeolite L as an example, we examine the factors such as seed layer deposition, secondary growth conditions, time and temperature on the growth of sub-micron to micron-sized membranes.

2. Experimental

Disk-shaped Linde type L zeolites were prepared from an opaque gel with the following composition: $5.4K_2O:5.7Na_2O:1Al_2O_3:30SiO_2:500H_2O$. Nanocrystalline Linde type L zeolites were synthesized from a clear solution with the following composition: $10K_2O:1Al_2O_3:20SiO_2:400H_2O$. The influence of chemical composition on the morphology of zeolite L (LTL) seed crystals is described in the literature [16,19–23]. The sodium/potassium aluminate solution was prepared by dissolving aluminum hydroxide (Alfa Aesar, 80.5%) in an alkaline solution of sodium hydroxide (Mallinckrodt, 98.8%) and/or potassium hydroxide (GFS Chemicals, 85%) prepared from doubly distilled water. Both the aluminate and silicate (Ludox HS-40 (disk), Ludox LS-30 (nano), Aldrich) solutions were sonicated for 20 min prior to mixing with vigorous stirring. In the case of the disk-shaped zeolites, the thick gel was placed into a 125 mL Teflon-lined Parr general purpose digestion vessel and heated using static conditions at 170 °C for 70 h prior to quenching in cold water. Nanocrystalline zeolite L were produced by rotating (16 rpm) a 25 mL digestion vessel at 170 °C for 6 h. To prevent agglomeration, the zeolite seed crystals were neutralized with distilled water and stored as an aqueous stock suspension (0.054 g/mL for disk, 0.08 g/mL for nano) for the preparation of zeolite L seed layers by dip-coating technique.

The macro-porous supports, upon which the zeolite membranes were grown, were prepared by sintering of $\alpha-Al_2O_3$ colloidal casting compacts at 1050 °C. This procedure leads to a surface pore size of 40–60 nm, a porosity of 33%, a surface roughness of ~ 20 nm and a He perme-

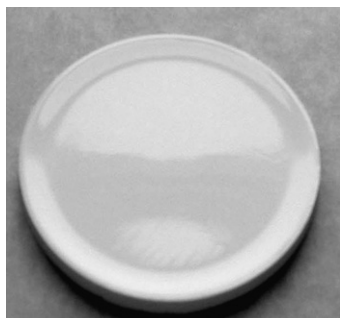


Fig. 1. Top-view of 42 mm, optically smooth α -alumina support.

ance of $2.8 \times 10^{-6} \text{ kmol m}^{-2} \text{ s}^{-1} \text{ kPa}^{-1}$. A surface view of a 42 mm diameter, defect free, optically smooth support is provided in Fig. 1, which illustrates the large workable surface for seed layer deposition/membrane formation. Detailed information about support preparation has been described elsewhere [24].

Zeolite L seed layers were deposited on the alumina supports by dip-coating with a MEMDIP coating unit (Pervatech BV, The Netherlands), using the zeolite dispersions described below. Throughout this entire study, seed layers were deposited from a single dip-coating cycle. The starting solution for the dip-coating process was prepared by mixing disk-shaped or nanocrystalline zeolite L particles into an aqueous solution of polyethyleneimine (PEI), having an average molecule weight of 1800 Daltons. Using a 0.5–1 wt% solution of PEI in water, a 0.95–2.03 mg/mL dispersion of disk-shaped LTL (0.08–2.0 mg/mL for nanocrystallites) was prepared in an ultrasonic bath for 1 h. Throughout the sonication, the temperature of the dispersion was maintained below 20 °C. During dip-coating, the substrate was withdrawn at a speed of 0.01 m/s from a watchglass filled with 15 mL of the zeolite suspension. The zeolite L seed layers were dried overnight at approximately 40 °C and then fired in air at a temperature of 500 °C (0.5 °C/min heat/cool rate) to remove the organic polymers. The integrity and thickness of the zeolite seed layer remained unaffected by this firing procedure, as confirmed with X-ray diffraction.

The supported zeolite seed layers were converted into membranes using hydrothermal secondary growth. The secondary growth solution used was adapted from a previous report of secondary growth on unsupported zeolite L films [15,16]. A clear solution was prepared with a molar composition of $10K_2O:1Al_2O_3:20SiO_2:2000H_2O$. The aluminate and silicate (Ludox LS-30, Aldrich) solutions were sonicated for 15 min prior to mixing. The secondary growth solution was vigorously stirred for 15 min. Suspended in a 125 mL Teflon-lined Parr digestion vessel, the membranes were grown by placing the films vertically in the secondary growth solution (filled to 80% of total vessel volume). To optimize secondary growth conditions (temperature and time), the synthesis temperatures were varied from 110 to 175 °C with times of 20–90 h. At least three membranes were prepared at each growth time and temperature to support the experimental findings.

Phase composition of zeolite materials was determined with a Rigaku Geigerflex X-ray diffractometer using nickel-filtered $Cu K\alpha$ ($\lambda = 1.5405 \text{ \AA}$) radiation. The zeolite membrane surface morphology was investigated by scanning electron microscopy (JEOL JSM-5500, JEOL, Tokyo, Japan) on carbon or gold coated specimens. In addition, membrane densification and thickness were investigated by SEM of fracture cross-sections of the supported membrane structure.

The thickness of the nanocrystalline zeolite L seed layers was verified non-destructively with a vertically oriented variable angle spectroscopic ellipsometer (V-VASE, J.A.

Woollam Co. Inc., Lincoln, NE). As homogeneous, dense packed, nanocrystalline zeolite L is optically transparent, the dispersion in refractive index, n , can be described as a Cauchy type material with the following equation:

$$N^2 = c_1 + c_2/\lambda^2 + c_3\lambda^2 \quad (1)$$

Here λ is the wavelength of the light and c_1 , c_2 , and c_3 are fitting parameters. The optical constants of the porous α -alumina supports were determined prior to analyzing the zeolite layer in order to accurately characterize the ellipsometric response from the thin zeolite films. VASE analysis of the bare supports exhibit absorption in the visible region of the spectrum due to light scattering from the surface and/or near bulk. This absorption is represented by a generalized oscillator model consisting of a single Tauc–Lorentz type oscillator. The index is then matched using a pole in the ultraviolet and an offset to the Kramers–Kronig transformation of the absorption [25].

Single gas permeation experiments were employed to investigate the optimum hydrothermal conditions in which dense, defect free zeolite L membranes could be achieved. These measurements were carried out in the non-stationary dead-end mode [26]. The supported membranes were mounted in a gas permeation cell and evacuated under vacuum at 80 °C overnight prior to applying a permeate gas. As shown in Fig. 2, a constant pressure of test gas is supplied at the feed side. Gas passes through the compact into a pre-evacuated reservoir with volume V_{cell} . The feed and permeate pressure, respectively, p_f^0 and p_p , are measured with a pressure transducer (model PX303-200G10V Omega Engineering, Inc., USA). Assuming the ideal gas law to be valid, the gas permeance, f , is determined for isothermal conditions by non-linear regression using the following equation:

$$\ln(p_f^0/p_f - p_p) = f(A/X)(RT/V_{\text{cell}})t \quad (2)$$

where A is the apparent membrane surface, X the support thickness, R the gas constant, T the absolute temperature, and t the relative time. This setup is capable of measuring gas permeance values as low as 10^{-13} kmol m⁻² s⁻¹ kPa⁻¹.

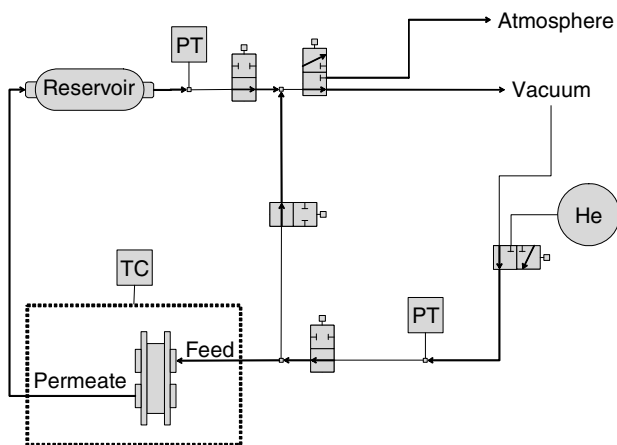


Fig. 2. Diagram of the non-stationary single gas permeation setup.

3. Results and discussion

Q1

3.1. Micron-thick membranes

3.1.1. Seed layer deposition

Zeolite L with disk-like morphology was synthesized using a static hydrothermal technique. The scanning electron micrograph in Fig. 3 suggests that crystals ranging primarily from 0.5 to 2 μm in diameter and comparable thicknesses are being formed. X-ray diffraction was used to characterize the crystallinity of the zeolite and also confirmed that no impurity phases were present (data not shown).

Zeolite membranes are most commonly obtained by hydrothermal secondary growth of an existing seed layer on a support [27–34]. The zeolite seed layer is critical in determining the quality of membrane produced; therefore, the morphology of the seed crystallites and their extent of agglomeration determine the quality of the membrane. Several techniques for seed layer deposition are currently available, which include: rubbing [27–29,35], spin coating [36,37], electrostatic adsorption [30,32,33,38–40], electrophoretic deposition [41–43], and dip coating [27,31,33]. Due to the existence of relatively high capillary forces, dip-coating has been found appropriate for producing uniform seed layers with optimum adhesion. This method is also preferred for practical applications since it does not require time-consuming and costly surface pre-treatment of support and/or particles [27,33].

In order to prevent agglomeration of the zeolites, various polymers such as polyvinyl alcohol (PVA), polyvinyl pyrrolidone (PVP), and polyethyleneimine (PEI) were added to the zeolite suspensions. Polymers ranging from 1 to 5 wt% were used. It was found that PVA and PVP did not improve the surface coverage when compared to

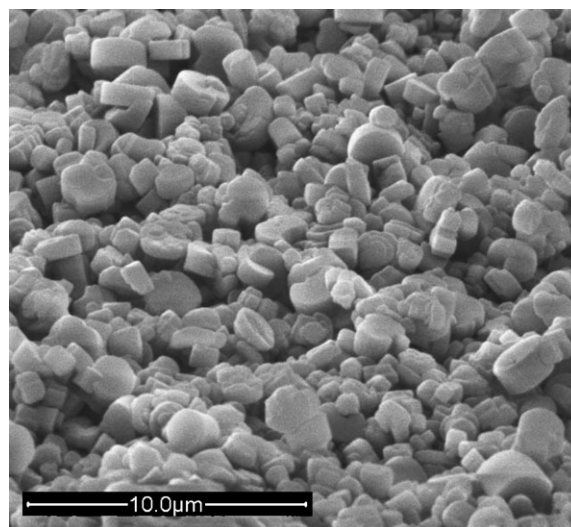


Fig. 3. SEM image of the disk-like zeolite L crystals following dip-coating with a 2.03 mg/mL zeolite suspension (1 wt% PEI) onto the α -alumina supports prior to secondary growth.

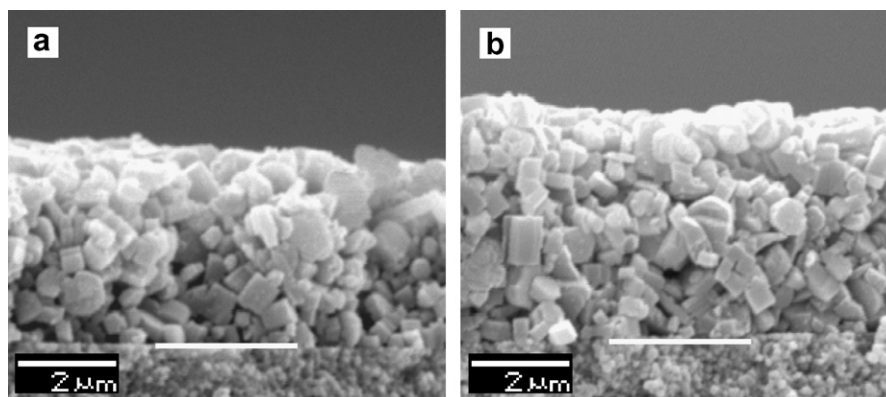


Fig. 4. SEM cross-sections of seed layers prepared from different zeolite concentrations using 1 wt% PEI. (a) $\sim 3.8 \mu\text{m}$ layer from 1.35 mg/mL suspension, (b) $\sim 5.1 \mu\text{m}$ layer from 2.03 mg/mL suspension (white bar shows demarcation between zeolite seed layer and support).

dip-coatings performed without polymer addition. However, as shown in Fig. 3, 1 wt% PEI was shown to provide good surface coverage of the alumina support. Fig. 3 also illustrates that the particle size distribution is advantageous for generating continuous films in that the smaller crystals can fill in the large interzeolite gaps. Little improvement was observed when the concentration of polymer was increased to 5 wt%.

The zeolite concentration of the dipping solution determined the seed layer thickness. As demonstrated by the SEM cross-sections in Figs. 4a and b, the zeolite seed layer thickness was tuned by changing the solid load of the dipping solution. The $\sim 3.8 \mu\text{m}$ seed layer in Fig. 4a was prepared from a 1.35 mg/mL zeolite concentration, while a concentration of 2.03 mg/mL provides a $\sim 5.1 \mu\text{m}$ zeolite layer shown in Fig. 4b. When the zeolite concentration is lowered to 0.95 mg/mL, the thickness is reduced to $\sim 2.76 \mu\text{m}$ (discussed later in results). SEM was used to examine the zeolite coverage of the alumina supports for these three dipping suspensions, with Fig. 3 being an example of a completely covered support using the 2.03 mg/mL dipping solution. These well-stabilized zeolite suspensions have also proven useful, in that uniform seed layers as large as 1133 mm^2 are deposited on the support. This dip-coating procedure can be generalized for seeding larger supports, as well as the preparation of uniform seed layers using many zeolite types.

3.1.2. Secondary growth

Tsapatsis et al. reported a growth solution comprised of $10\text{K}_2\text{O}:1\text{Al}_2\text{O}_3:20\text{SiO}_2:2000\text{H}_2\text{O}$ for secondary growth of nanocrystalline zeolite L seed crystals [16]. Using this growth solution, our supported zeolite films were subjected to various growth temperatures to maximize membrane densification and to minimize the formation of other phases. As demonstrated by SEM in Fig. 5a, secondary growth for 6 h at 175°C led to the formation of phillipsite [44], which becomes more evident at 24 h because the large phillipsite impurities covered the membrane surface (confirmed by XRD). At 150°C , phillipsite also began to develop after

6 h of secondary growth. Even at 130°C , the phillipsite impurity appeared between 6 and 10 h of growth. Fig. 5b is a SEM of a zeolite L seeded layer that has undergone secondary growth for 72 h at 110°C . As compared to Fig. 5a, the micrograph in Fig. 5b suggests a single phase, thus providing support that 110°C is the optimum temperature for zeolite growth. Decreasing the temperature below 100°C provided limited secondary growth, in which no densification of the zeolite seed layer was observed.

Using a set of five separately seeded zeolite films, the growth time was optimized by varying the time from 20 to 80 h. Each of these seed layers was prepared by using a 1.35 mg/mL zeolite suspension. Fig. 6(a–d) shows SEM images of these individually cross-sectioned zeolite membranes following the specified growth time at 110°C . At 20 h growth (Fig. 6a), individual zeolite crystals are still observed, despite the progression towards membrane densification. Zeolite intergrowth begins to occur, yet the intercrystalline pores between neighboring zeolites are still present. After 40 h growth (Fig. 6b), the individual zeolite crystals are difficult to recognize because of the increase in intergrowth. Membrane densification has increased from 20 h; however, the intercrystalline pores are not completely closed. According to the SEM micrographs, growth times greater than 60 h (Fig. 6c) produce zeolite L membranes that appear to be dense. As observed in Fig. 6d for 72 h growth time, zeolite intergrowth has made it almost impossible to resolve individual crystals and the intercrystalline pores that were previously observed are no longer visible. Growth times up to 90 h were utilized for these experiments; however, no major changes in the cross-sections were observed for times greater than 66 h. Despite the long growth time, no impurities were noted.

Upon closer examination of the cross-sections in Fig. 6, the average thickness of the zeolite membranes is $3.75 \pm 0.24 \mu\text{m}$ thick. Even after 72 h of growth, the thickness of the membrane does not change from that observed at 20 h growth. A second example of controlled thickness is provided in Fig. 7, in which seed layers were deposited onto separate supports from a 0.95 mg/mL zeolite suspension.

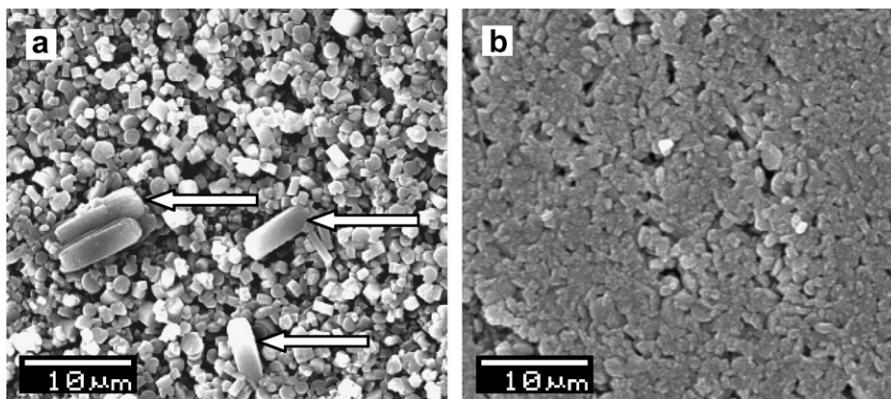


Fig. 5. SEM images of the surface of zeolite seeded layers after secondary growth at the specified times and temperatures (presence of phillipsite indicated by arrows). (a) 6 h at 175 °C and (b) 72 h at 110 °C.

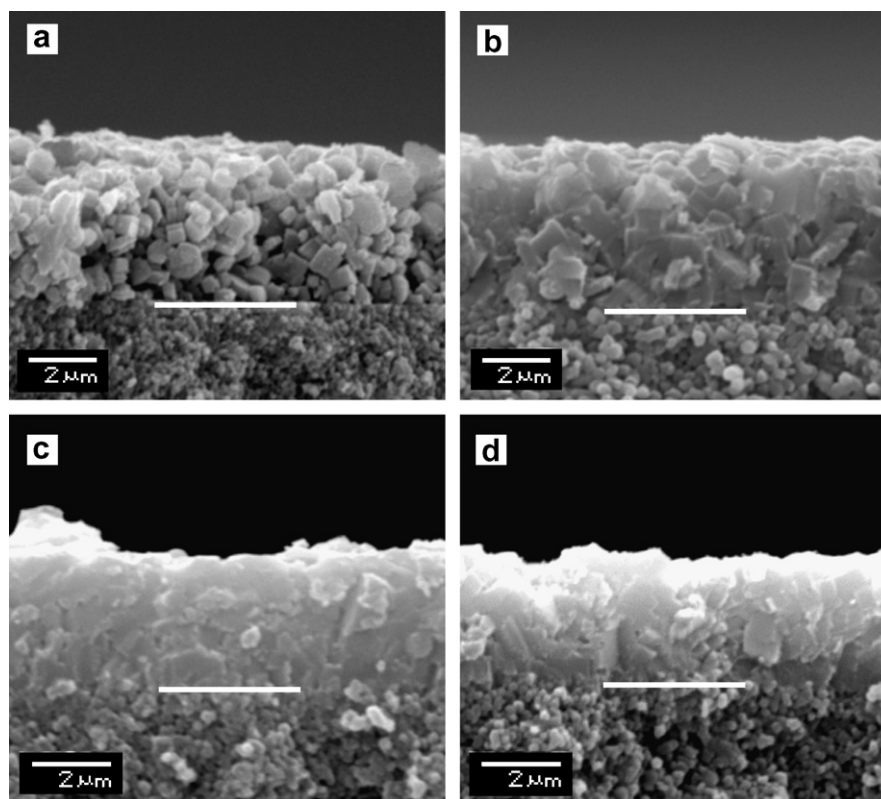


Fig. 6. SEM cross-sections (a–d) of zeolite L membranes formed at various secondary growth times at 110 °C. Seed layers prepared using 1.35 mg/mL suspension. (a) 20 h, (b) 40 h, (c) 66 h, and (d) 72 h. Dense membranes are observed at times from 60 h of secondary growth (white bar shows demarcation between zeolite membrane and support).

The SEM cross-sections show that the thickness remains the same with increasing growth time. Due to the reproducibility in preparing seed layers on multiple supports, a membrane thickness of $2.76 \pm 0.05 \mu\text{m}$ was obtained for the samples prepared from a 0.95 mg/mL zeolite suspension. Based on the experimental data, lowering the temperature to 110 °C reduces the vertical growth of the zeolite membranes so that densification only occurs inside the seed layer, thus maintaining the same thickness as deposited during seeding.

To further support the fact that secondary growth is limited to the xy -plane, the surface of every membrane from Fig. 6 was imaged following membrane densification. Fig. 8 illustrates that secondary growth is simply filling in the interzeolite pores. The surface view in Fig. 8a was collected prior to secondary growth, in which the boundaries of the zeolites are clearly defined because of the large interzeolite pores between them. However, after 72 h of growth in Fig. 8b, the interzeolite pores have begun to close, making it more difficult to resolve the individual crystals.

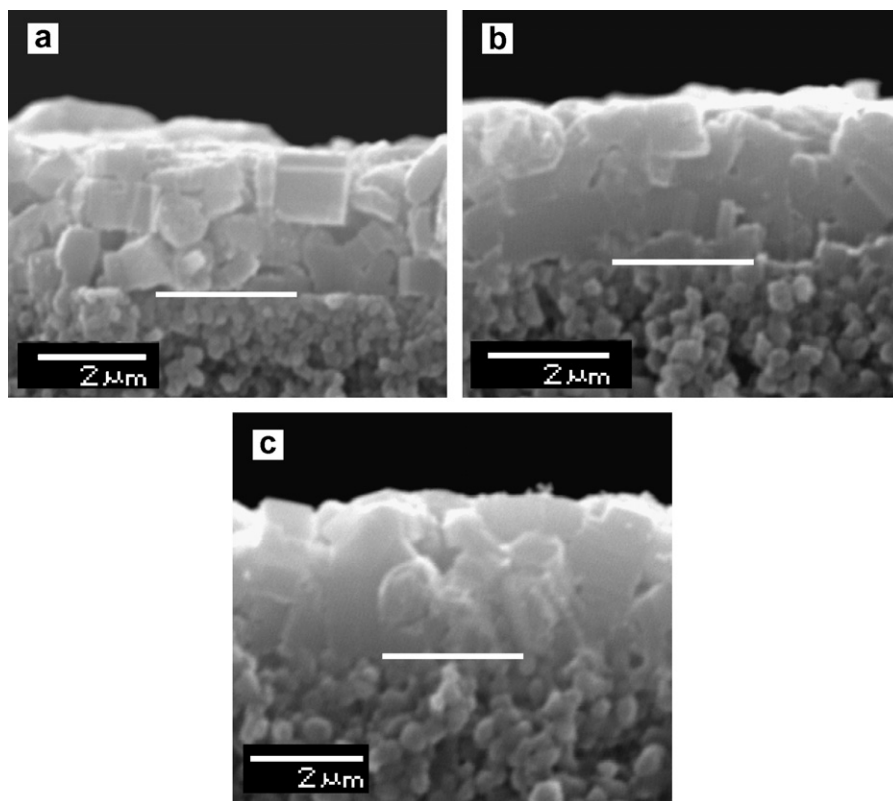


Fig. 7. SEM cross-sections of seed layers prepared from a 0.95 mg/mL zeolite solution and later grown into zeolite L membranes. (a) 20 h, (b) 40 h, and (c) 60 h. Minimal vertical growth was observed (white bar shows demarcation between zeolite membrane and support).

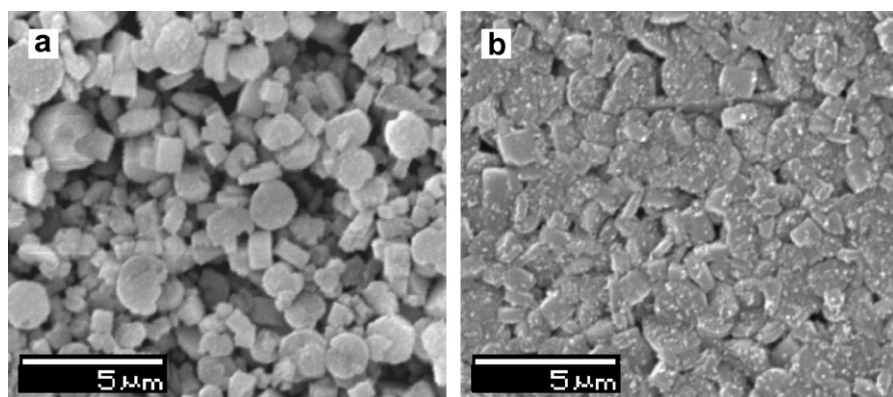


Fig. 8. SEM surface views of zeolite L seed layers at various secondary growth times at 110 °C. (a) 0 h and (b) 72 h.

The X-ray diffraction patterns in Fig. 9 were collected on a set of 3.75 μm zeolite membranes formed by secondary growth. The diffraction pattern represented by (a) was obtained on a seeded support prior to secondary growth. Patterns (b) and (c) were taken following 20 and 60 h of secondary growth, respectively. The inset in Fig. 9 compares the diffraction pattern of the randomly oriented zeolite L powder used for seeding (solid line) to a membrane grown after 60 h (dotted line). For the randomly oriented powder, the peak intensity at 5.5° 2θ (100) is approximately 3 times larger than the peak at 11.7° 2θ (001). In the case of the membranes, the peak

intensity ratio between these two peaks gets smaller, especially with longer growth time. As shown in the inset, the intensities of the (100) and (001) peaks are roughly the same height after 60 h of secondary growth. This supports the fact that there is some preferred orientation of the zeolites in the membrane along the (001) plane. There are also several peaks between 13° and 25° 2θ that have much lower intensities when compared to the randomly oriented powder. Collectively, these patterns provide evidence of the preferential orientation of the zeolite L crystals within the membrane following seed layer deposition and secondary growth.

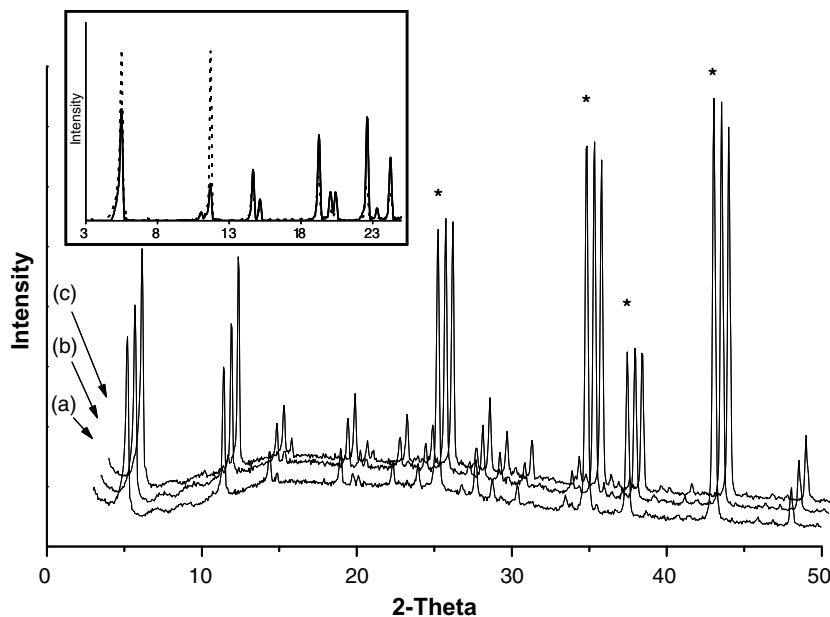


Fig. 9. Stacked X-ray diffraction spectra showing secondary growth of the zeolite L membranes at 110 °C with increasing growth time. (a) 0 h, (b) 20 h, and (c) 60 h. Diffraction peaks from α -alumina are denoted with an (*). Inset compares diffraction pattern of a randomly oriented zeolite L powder (solid line) to a membrane grown for 60 h (data baseline corrected).

3.1.3. Permeation measurements

Non-stationary single gas permeation was solely used to determine the integrity and densification of the 3.75 μm zeolite L membranes as a function of time. In Fig. 10, the permeate pressure of the reservoir (p_p) is plotted as a function of time for zeolite L membranes that were achieved at different secondary growth times. At initial time, t^0 , the reservoir was evacuated ($p^0 \sim 10$ kPa), and over time, He gradually fills the reservoir. The pressure closely follows the trend of Eq. (2), from which it can be concluded that the permeance does not have pressure dependence (see Fig. 10). Due to the design of the gas permeation cells and the operation temperature, the non-stationary gas permeation setup used has a detection limit of 10^{-12} – 10^{-14} $\text{kmol m}^{-2} \text{s}^{-1} \text{kPa}^{-1}$ due to desorption

and parasitic leaks. This was confirmed by using a dense aluminum plate with negligible He permeance.

Fig. 11 shows the overall f_{He} values for supported zeolite L membranes prepared using a 1.35 mg/mL solution and grown at different times. Increased growth time leads to a decrease in He permeance. For comparison, the helium permeance of a denser α -alumina support immersed into the growth solution for 72 h resulted in a permeance of 1.6×10^{-7} $\text{kmol m}^{-2} \text{s}^{-1} \text{kPa}^{-1}$. Despite inherently lower permeances of 2×10^{-7} $\text{kmol m}^{-2} \text{s}^{-1} \text{kPa}^{-1}$ for these bare supports when compared to the supports detailed in the paper, it was concluded that the permeance of the support was not affected by the secondary growth treatment. As the membrane growth time approached 60 h, a limiting permeance (10^{-9} $\text{kmol m}^{-2} \text{s}^{-1} \text{kPa}^{-1}$) was measured.

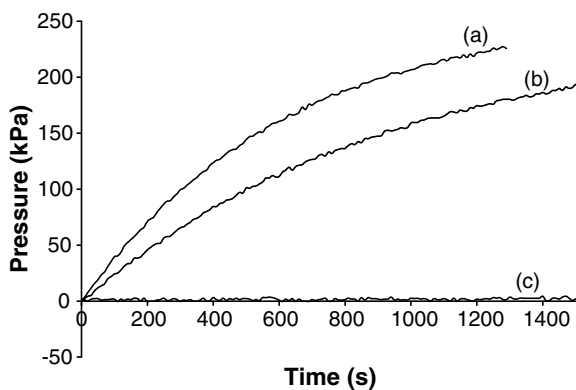


Fig. 10. Permeate pressure vs. time obtained for zeolite L membranes prepared at various secondary growth times. (a) 20 h, (b) 40 h, and (c) 80 h.

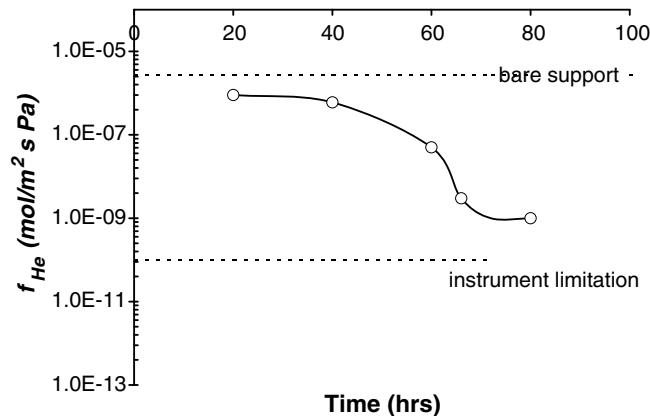


Fig. 11. Helium permeance of supported zeolite L membranes as a function of secondary growth time.

Single gas permeation supports the results from electron microscopy that membrane densification improves with increased secondary growth times due to the fact that helium becomes unable to penetrate through the zeolite membrane. Based on the (0.26 nm) kinetic diameter of He, the gas should easily penetrate the 0.71 nm pores of zeolite L; however, due to the orientation of the crystals, it is unlikely that a single one-dimensional pore from zeolite L spans its entire width. This implies that the absence of connected macro- and micro-defects in the supported membranes is confirmed by non-stationary single gas permeation.

3.2. Sub-micron thick membranes

3.2.1. Seed layer deposition

As shown above, the disk-like LTL crystallites of 0.5–2 μm are suitable for the preparation of membranes greater than one micron. In order to reduce the membrane thickness into the sub-micron regime, nanocrystalline zeolite L particles were utilized for making the initial seed layer. Nanocrystalline zeolite L was synthesized using a dynamic hydrothermal technique that produces crystals with a size of about 15 nm wide and 40 nm long, as revealed in the transmission electron micrograph in Fig. 12a. The X-ray diffraction pattern in Fig. 12b (solid line) confirmed that the particles were crystalline and smaller based on peak broadening when compared to the spectrum of micron-sized zeolite L (dotted line).

Just as in the case with the micron-sized zeolite L, membranes on alumina supports were prepared from the dipping of well-dispersed solutions of nanocrystalline zeolite L. Again, the zeolite seed layer is critical in determining the quality of the membrane after secondary growth. Due to the high surface energy of the nanoparticles, they tend to agglomerate into larger clusters (80–120 nm); therefore, the dipping solution was optimized using polymers to prevent agglomeration. A range of PEI and PVP (0.5–2 wt%) was used to disperse the particles, but PVP was found to

promote particle agglomeration into 300–400 nm clusters. PEI (0.5 wt%) was found to provide minimal particle agglomeration and good surface coverage of the alumina support was observed by SEM.

The zeolite concentration in the dipping solution determined the thickness of the deposited seed layer. Ellipsometry data shown in Fig. 13 indicates that the thickness of the zeolite L seed layer can be tuned from 150 to 2000 nm by changing the zeolite concentration from 0.08 to 2.0 mg/mL. This plot indicates the linearity in the seed layer deposition with respect to zeolite concentration. Several examples of the as prepared nanocrystalline zeolite L seed layers are provided in the side and top-view SEM images shown in Fig. 14. These images provide confirmation of the seed layer thicknesses determined by spectroscopic ellipsometry. A non-continuous film generated from a 0.08 mg/mL solid load is shown in Fig. 14a and b. Fig. 14c and d shows a continuous 330–350 nm thick film, which was deposited using a 0.4 mg/mL zeolite concentration. The 1.2 μm thick seed layer in Fig. 14e and f was generated from a 2.0 mg/mL dipping solution. As concluded from SEM, the seed layer is not continuous below 0.4 mg/mL.

3.2.2. Secondary growth

Utilizing the same secondary growth solution and procedure previously described for the micron-sized membranes, the nanocrystalline zeolite L seed layers prepared using 0.4–2 mg/mL dipping solutions were subjected to hydrothermal secondary growth. Fig. 15 provides SEM images of a nanocrystalline zeolite L membrane (1.0 mg/mL) following 48 h growth time at 110 $^{\circ}\text{C}$. As observed in Fig. 15, the zeolite intergrowth after 48 h has fused neighboring particles to create what appears to be a dense zeolite L membrane.

Fig. 15 provides an example of a nanocrystalline zeolite L membrane that was prepared using a 1.0 mg/mL solid load, which provides a seed layer thickness of approximately 650 nm. Upon close examination of the cross-section

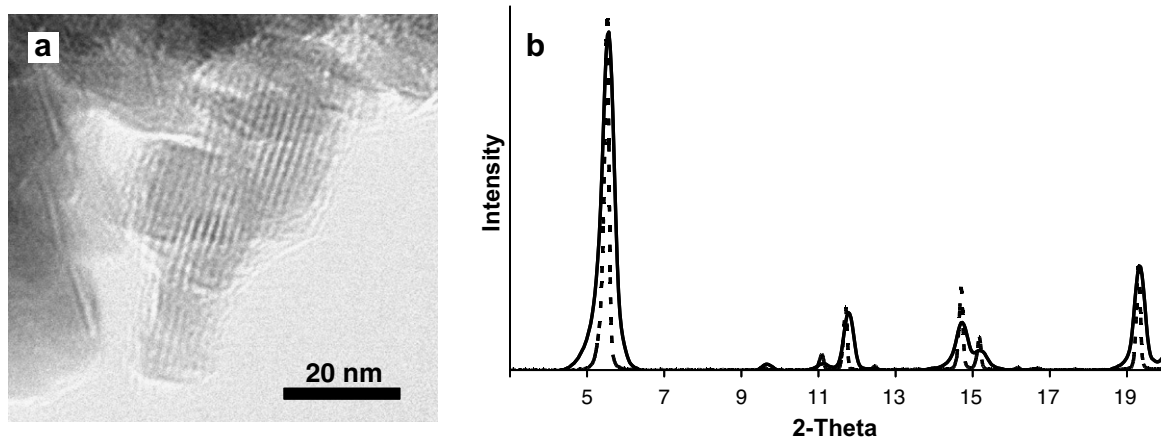


Fig. 12. (a) Transmission electron micrograph of nanocrystalline zeolite L. (b) Normalized X-ray diffraction pattern of nanocrystalline zeolite L (solid line) compared to micron-sized zeolite L (dashed line) (baseline corrected).

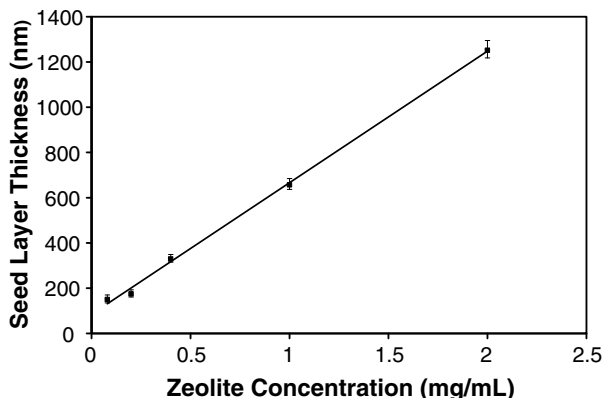


Fig. 13. Plot showing the linearity of the nanocrystalline zeolite L seed layer thickness versus the zeolite concentration of the dipping solution, as determined by spectroscopic ellipsometry.

tion, the membrane has grown to approximately 1050 nm. Unlike the thickness of the micron-sized membranes remaining unchanged, the experimental data suggests that the nanocrystalline membranes almost double in thickness during secondary growth. After examining all nanocrystalline membranes by SEM, our findings indicate that one requires a dipping solution that deposits a zeolite layer greater than 350 nm and the final membrane thickness needs to be greater than 700 nm in order to create a uniform nanocrystalline zeolite L membrane.

3.2.3. Permeation measurements

Non-stationary single gas permeation was used to characterize the nanocrystalline zeolite L membrane (1.0 mg/mL solution) shown in Fig. 15. Using helium as the perme-

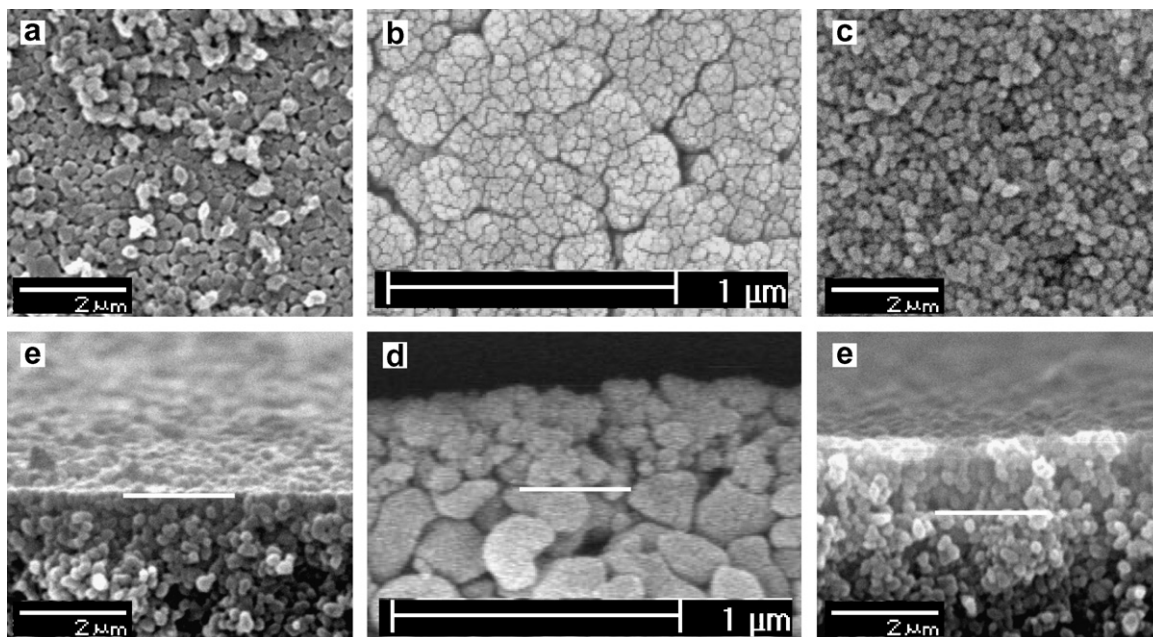


Fig. 14. SEM top-view and cross-sections of nanocrystalline zeolite L seed layers using 0.5 wt% PEI at various concentrations. (a, b) 0.08 mg/mL; (c, d) 0.4 mg/mL; (e, f) 2.0 mg/mL (white bar shows demarcation between zeolite seed layer and support).

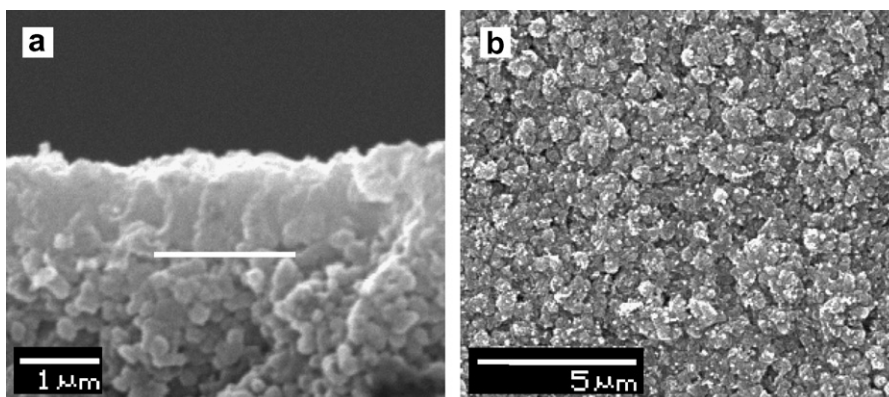


Fig. 15. SEM top-view and cross-section of a dense, nanocrystalline zeolite L membrane after 48 h of secondary growth. Seed layer was deposited using a 1.0 mg/mL suspension (white bar shows demarcation between zeolite membrane and support).

ate gas, the membrane was found to have a limiting permeance from 1 to 5×10^{-9} kmol m⁻² s⁻¹ kPa⁻¹ when cycled from 30 to 180 °C at 50 °C intervals. X-ray diffraction of the thin membrane provides very weak peaks, yet enough to suggest that preferred orientation of the crystals is not occurring (data not shown). Due to the random orientation of the zeolites within the membrane, low permeance values were expected. A membrane prepared using a 0.2 mg/mL solid load was found to have a much higher permeance of $2\text{--}4 \times 10^{-7}$ kmol m⁻² s⁻¹ kPa⁻¹ and is due to insufficient surface coverage, thus an incomplete zeolite membrane. This data is consistent with the SEM images of the seed layers, in that complete surface coverage can be obtained using zeolite concentrations of 0.4 mg/mL or higher. These helium permeances are consistent with the values obtained for the micron-sized membranes grown at 60 h or more, thus supporting the fact these supported membranes are absent of connected macro- and micro-defects.

4. Conclusions

Zeolite L of disk-like and nanocrystalline morphology has been successfully dip-coated onto macro-porous alumina supports and grown into homogeneous, dense membranes, ranging from 0.7 to 5.1 μm thick, using a hydrothermal secondary growth process. Through the use of stabilized zeolite suspensions, uniform zeolite seed layers of a desired thickness were prepared. Optimal secondary growth conditions were determined in order to minimize the growth of impurities, while at the same time, densifying the zeolite films laterally without changing their initial thicknesses. For the disk-shaped zeolites, secondary growth times above 60 h yield dense membranes, as demonstrated with SEM cross-sections and confirmed with single gas permeation experiments. With nanocrystalline zeolite L as seed layers, membranes were formed above 48 h of growth time, which was also confirmed using the same techniques. The strategies for the preparation of zeolite membranes discussed in the present study could be successfully applied for a wide range of other zeolite types by tuning the experimental conditions to produce dense, controlled thickness, defect free membranes.

Acknowledgments

This work was supported by The Basic Research for the Hydrogen Fuel Initiative Program (DOE, grant No. DF-FG01-04FR04-20). We also thank the reviewers for helpful comments.

References

- [1] J.A. Rabo, M.L. Poutsma, *Adv. Chem. Ser.* 102 (1971) 284.
- [2] G.V. Tsitsishvili, *Adv. Chem. Ser.* 121 (1973) 291.
- [3] D.W. Breck, R.W. Grose, *Adv. Chem. Ser.* 121 (1973) 319.

- [4] J.C. Yang, P.K. Dutta, *Sensors Actuators B* 123 (2007) 929.
- [5] Y. Kim, A. Das, H. Zhang, P.K. Dutta, *J. Phys. Chem. B* 109 (2005) 6929.
- [6] S. Megelski, G. Calzaferri, *Adv. Funct. Mater.* 11 (2001) 277.
- [7] J.M. van de Graaf, E. van der Bijl, A. Stol, F. Kapteijn, J.A. Moulijn, *Ind. Eng. Chem. Res.* 37 (1998) 4071.
- [8] Y. Yan, M.E. Davis, G.R. Gavalas, *J. Membrane Sci.* 123 (1997) 95.
- [9] J. Coronas, R.D. Noble, J.L. Falconer, *Ind. Eng. Chem. Res.* 37 (1998) 166.
- [10] M. Tsapatsis, G. Xomeritakis, A. Gouzinis, S. Nair, T. Okubo, M. He, R. Overney, *Chem. Eng. Sci.* 54 (1999) 3521.
- [11] Y. Yan, M.E. Davis, G.R. Gavalas, *J. Membrane Sci.* 126 (1997) 53.
- [12] L.Y. Au, W.Y. Mui, P.S. Lau, C.T. Ariso, K.L. Yeung, *Micropor. Mesopor. Mater.* 47 (2001) 203.
- [13] D.W. Breck (Ed.), *Zeolite Molecular Sieves*, Wiley, New York, 1974.
- [14] W.M. Meier, D.H. Olsen, C. Bärlocher (Eds.), *Atlas of Zeolite Structure Types*, Elsevier, London, 1996, p. 229.
- [15] M. Tsapatsis, M. Lovallo, *Chem. Mater.* 8 (1996) 1579.
- [16] M.C. Lovallo, M. Tsapatsis (Eds.), *Nanocrystalline Zeolites. Synthesis, Characterization, and Applications with Emphasis on Zeolite L Nanoclusters*, Academic, San Diego, CA, 1996, p. 307.
- [17] P.K. Dutta, Y. Kim, *Curr. Opin. Solid State Mater. Sci.* 7 (2003) 483.
- [18] P.K. Dutta, Y. Kim, *J. Phys. Chem. C* 111 (2007) 10575.
- [19] A.Z. Ruiz, D. Bruhwiler, T. Ban, G. Calzaferri, *Monatsh. Chem.* 136 (2005) 77.
- [20] Y.J. Lee, J.S. Lee, K.B. Yoon, *Micropor. Mesopor. Mater.* 80 (2005) 237.
- [21] Y.S. Ko, W.S. Ahn, *Powder Technol.* 145 (2004) 10.
- [22] O. Larlus, V.P. Valtchev, *Chem. Mater.* 16 (2004) 3381.
- [23] Y.S. Ko, W.S. Ahn, *Bull. Kor. Chem. Soc.* 20 (1999) 1.
- [24] K. Shqau, M.L. Mottern, D. Yu, H. Verweij, *J. Am. Ceram. Soc.* 89 (2006) 1790.
- [25] M.L. Mottern, K. Shqau, F. Zalar, H. Verweij, *J. Membrane Sci.* (2007).
- [26] Y.S. Lin, A.J. Burggraaf, *J. Membrane Sci.* 79 (1993) 65.
- [27] X. Gu, J. Dong, T.M. Nenoff, *Ind. Eng. Chem. Res.* 44 (2005) 937.
- [28] F. Bonhomme, M.E. Welk, T.M. Nenoff, *Micropor. Mesopor. Mater.* 66 (2003) 181.
- [29] K. Kusakabe, T. Kuroda, A. Murata, S. Morooka, *Ind. Eng. Chem. Res.* 36 (1997) 649.
- [30] M. Lassinanti, J. Hedlund, J. Sterte, *Micropor. Mesopor. Mater.* 38 (2000) 25.
- [31] M. Pan, Y.S. Lin, *Micropor. Mesopor. Mater.* 43 (2001) 319.
- [32] L. Tosheva, V.P. Valtchev, *C.R. Chim.* 8 (2005) 475.
- [33] L.C. Boudreau, J.A. Kuck, M. Tsapatsis, *J. Membrane Sci.* 152 (1999) 41.
- [34] X. Xu, W. Yang, J. Liu, L. Lin, *Micropor. Mesopor. Mater.* 43 (2001) 299.
- [35] B.H. Jeong, K.I. Sotowa, K. Kusakabe, *J. Membrane Sci.* 224 (2003) 151.
- [36] Z.B. Wang, A. Mitra, H.T. Wang, L.M. Huang, Y. Yan, *Adv. Mater.* 13 (2001) 1463.
- [37] S. Mintova, T. Bein, *Adv. Mater.* 13 (2001) 1880.
- [38] J. Hedlund, J. Sterte, M. Anthonis, A.J. Bons, B. Carstensen, N. Corcoran, D. Cox, H. Deckman, W.D. Gijnst, P.P. de Moor, F. Lai, J. McHenry, W. Mortier, J. Reinoso, J. Petersl, *Micropor. Mesopor. Mater.* 52 (2002) 179.
- [39] W. Yang, X. Wang, Y. Tang, Y. Wang, C. Ke, S. Fu, *J. Macromol. Sci. Pure Appl. Chem.* 39 (2002) 509.
- [40] Y. Wang, Y. Tang, X. Wang, W. Shan, C. Ke, Z. Gao, J. Hu, W. Yang, *J. Mater. Sci. Lett.* 20 (2001) 2091.
- [41] C. Ke, W.L. Yang, Z. Ni, Y.J. Wang, Y. Tang, Y. Gu, Z. Gao, *Chem. Commun.* (2001) 783.
- [42] T. Seike, M. Matsuda, M. Miyake, *Solid State Ionics* 151 (2002) 123.
- [43] T. Seike, M. Matsuda, M. Miyake, *J. Mater. Chem.* 12 (2002) 366.
- [44] A. Cichocki, J. Grochowski, L. Lebioda, *Krist. Tech.* 14 (1979) 9.